Available online at www.sciencedirect.com
ScienceDirect
Journal of Solid State Chemistry 180 (2007) 3049–3057
JOURNAL OF SOLID STATE CHEMISTRY
www.elsevier.com/locate/jssc

Structural investigations of sol–gel-derived $LiYF_4$ and $LiGdF_4$ powders

S. Lepoutre[a], D. Boyer[a,*], A. Potdevin[a], M. Dubois[a], V. Briois[b], R. Mahiou[a]

[a]*Laboratoire des Matériaux Inorganiques, CNRS UMR 6002, Université Blaise Pascal et Ecole Nationale Supérieure de Chimie de Clermont-Ferrand, 24 Avenue des Landais, 63177 Aubière cedex, France*

[b]*Synchrotron SOLEIL, L'Orme des Merisiers, BP48, 91192 Gif-sur-Yvette Cedex, France*

Received 7 June 2007; received in revised form 28 August 2007; accepted 6 September 2007
Available online 14 September 2007

Abstract

A soft synthesis route based on the sol–gel process was used for preparing rare-earth tetrafluoride powders from alkoxide precursors. In-situ fluorination was performed by decomposition of a fluorine containing organic compound named 1,1,1-trifluoro-5-methyl-2, 4-hexanedione when sintering the as-prepared xerogel to produce crystallized samples. Both to insure complete departure of organic residues as well as to avoid any oxidation into oxyfluoride, annealing treatment was carried out under fluorine atmosphere. Free-oxygen content of resulting samples was evidenced by infrared and Raman spectroscopies. X-ray absorption spectroscopies (XAS) and ^{19}F nuclear magnetic resonance (NMR) studies showed that samples heat treated at 300 °C are already crystallized but for a full crystallization in $LiGdF_4$ and $LiYF_4$ a thermal treatment at 550 °C is needed. Temperature dependence of powder morphology was analyzed by scanning electron microscopy (SEM).

Keywords: Sol–gel; Fluoride; 19F NMR; XAS

1. Introduction

Sol–gel processing of inorganic materials has become an area of intense researches because of inherent advantages compared with more conventional synthesis methods [1,2]. Starting from molecular precursors [3,4], e.g. metal alkoxides or inorganic salts, the sol–gel process is a convenient way to produce at low-temperature high-purity materials with chemical homogeneity even on the molecular scale. Moreover, due to the rheological properties of sols, this synthesis route allows a shaping versatility (fibers, powders, coatings and monoliths). Nevertheless, so far most inorganic compounds based on the sol–gel process consist only of oxide networks.

This paper is devoted to the development of a new class of mineral matrices through the sol–gel route, namely fluoride materials. When doped with rare-earth ions, these compounds exhibit outstanding luminescent properties [5] due to peculiar features: a wide band gap, a low nephelauxetic effect in addition to a moderate crystal field splitting, long lifetimes of excited levels of $4f^N$ configurations, and eventually low phonon energies. As a result, they are involved in devices belonging to a wide range of optical applications such as lasers [6], scintillators [7], energy storage or amplifiers.

Fujihara et al. have already proposed a multi-step procedure for synthesizing fluorides and oxyfluorides through the sol–gel method using metal alkoxides and trifluoroacetic acid as precursors [8,9]. But the main drawback of sol–gel-derived materials results from the presence of residual organic species such as O–H and C–H groups, which are sources of extrinsic phonons so that optical efficiencies are greatly affected and drop drastically. Thus, to overcome such an inconvenient, another synthesis way utilizing lanthanide salts for preparing rare-earth alkoxides and a β-diketone containing fluorine as in-situ fluorination agent was investigated [10–12]. This latter reagent is also utilized as stabilizing agent in the case of coating achievements. To prevent any oxidization and insure complete burning of organic groups, thermal treatments were performed under F_2 atmosphere.

*Corresponding author. Fax: +33 4 73 40 71 08.
E-mail address: damien.boyer@univ-bpclermont.fr (D. Boyer).

0022-4596/$ - see front matter © 2007 Elsevier Inc. All rights reserved.
doi:10.1016/j.jssc.2007.09.008

Following this procedure, $LiYF_4$ and $LiGdF_4$ powders were synthesized. Analyses of infrared and Raman spectroscopies were carried out to check the presence of any remaining residual organic group. Furthermore, structural arrangement from amorphous to crystallized samples was studied by X-ray diffraction (XRD), ^{19}F nuclear magnetic resonance (NMR) and X-ray absorption spectroscopies (XAS). Finally, morphology of samples heat treated at different temperatures was observed by scanning electron microscopy (SEM).

2. Experimental section

2.1. Samples preparations

All experiments were carried out under a free-moisture atmosphere to prevent any alteration of starting materials and intermediate chemical reagents during the synthesis procedure. Depending on the final composition, a heterometallic alkoxides solution was prepared by dissolving either anhydrous yttrium (1 eq.—Aldrich) or gadolinium (1 eq.—Aldrich) and lithium (1 eq.—Aldrich) chlorides in anhydrous isopropanol (^{i}PrOH-Acros), then by adding, under vigorous stirring, a solution of potassium isopropoxide obtained from metallic potassium (3 eq.—Aldrich) dissolved in ^{i}PrOH. The reaction was exothermic and immediate precipitation of potassium chloride was observed. After a 1 h reflux at 85 °C, 1,1,1-trifluoro-5-methyl-2,4-hexanedione (4/9 eq.—Aldrich) was introduced and a homogeneous solution was obtained after further refluxing for 4 h under stirring. After cooling, KCl was removed by centrifuging and a clear solution was isolated. A xerogel was obtained after drying the sol at 80 °C (15 h) and thereafter crystallized specimens of $LiGdF_4$ and $LiYF_4$ were produced by further sintering at 550 °C for 20 h in fluorine reactive atmosphere. In order to investigate the temperature dependence of the structural arrangement, intermediary samples were annealed at 300 °C for 20 h under the same conditions. Xerogels annealed under air atmosphere lead as well to fluorine compounds but in most cases unwanted oxyfluoride phases are also formed.

2.2. Experimental methods

XRD measurements were carried out on a Siemens D500 diffractometer operating with Cu$K\alpha$ radiations. The infrared spectra were recorded on a Nicolet 5700 FTIR spectrometer with the KBr pellet technique. Raman study was performed on a T64000 Jobin Yvon confocal microRaman spectrometer equipped with an Olympus microscope and with a CCD detector cooled with liquid nitrogen. The 514.532 nm line of a coherent Innova Ar 70C5 Laser operating at 100 mW emission power was used.

NMR experiments were performed on a Bruker AVANCE300 spectrometer operating at 282.2 MHz for ^{19}F nucleus. Two NMR Bruker probes were used: a static and a special magic angle spinning (MAS) probes operating with a 4 mm rotor. MAS spectra were performed with a spinning rate of 14 KHz using a simple sequence (τ-acquisition). The processing and acquisition parameters were 20 s recycle time and 4 μs single $\pi/2$ pulse duration. ^{19}F chemical shifts were referenced with respect to $CFCl_3$. Spin-lattice relaxation time T_1 was measured using a saturation-recovery sequence.

Yttrium K-edge and gadolinium L_3-edge EXAFS spectra of references and samples were collected at the Elettra Sincrotrone (Trieste, Italy) on the beamline BL-11-1 of the storage ring operating at 2/2.4 GeV with an optimal current around 300 mA. Measurements were performed at the Y K-edge (17,080 eV) and Gd L_3-edge (7243 eV) using a Si(111) double crystal monochromator. All data were recorded at liquid nitrogen temperature (77 K) in transmission mode using two ionization chambers filled with a mixture of nitrogen and argon optimized in pressure at each edge in order to achieve absorptions of 20% and 80% for incident I_0 and transmitted I_1 photon flux, respectively. At both edges, EXAFS spectra were collected with a step of 3 eV each 2 s. Typically, three or four scans were recorded from each sample to get a good signal over noise ratio. The powdered samples, finely grinded with boron nitride were prepared in shape of pellets whose thickness was chosen so that the absorption jump at the edge was close to 1. The pellets were sandwiched between two Kapton® adhesives tapes.

XAFS analysis was done using Sixpack [13] following this procedure. First, three or four spectra were averaged before being converted from energy to k space by setting E_0 (using the second derivative of the raw spectra to determine the inflection point in the edge) and fitting linear and low-order polynomial functions to the pre-edge and the post-edge regions, respectively. Then, the data were Fourier transformed using k^3 ponderation and an appropriate Kaiser Bessel window leading to the pseudo-radial distribution functions (PRDF). Besides, the software package ATOMS [14] and FEFF6l [15] were used to generate ab-initio phases and amplitude functions for single and multiple scattering paths in yttrium and gadolinium fluorides ($LiYF_4$, $LiGdF_4$, YF_3 and GdF_3) [16–19]. Using as components the data obtained from references and from amorphous phases (xerogels), linear least-squares fitting of k^3-weighted experimental EXAFS spectra of samples sintered at 300 °C were performed. They provided fractional contributions of each component spectrum to the experimental spectrum and have been used to monitor the final fitting of these samples. Generally, the precision of these linear fittings is told to be between ±5% and ±10% considering the data quality [20]. Their accuracy can be assessed by the minimization of the χ^2_V parameter [21].

Eventually, first shell EXAFS fitting was done with the Sixpack interface to IFEFFIT [21] using least-square refinements. This fitting leads to the determination of the structural parameters R (average atomic distance from the absorbing atom), N (number of atoms in the coordination

shell) and σ (Debye Waller factor) with an accuracy of 1%, 10% and 20%, respectively. The reliability of the fit could be assessed by a residual factor R_F, which has to be minimized [22].

Micrographs were collected using a Zeiss EVO 50 Scanning Electron Microscope operating at 5 kV.

3. Results and discussion

The XRD patterns recorded from the xerogel and annealed powders prepared by the sol–gel processes are shown in Figs. 1 and 2, respectively for yttrium and gadolinium based fluorides. One can see for both samples the increase of their crystallization with the sintering temperature. Prior to any thermal treatment, the XRD patterns of the as-prepared powders reveal an amorphous structure (Figs. 1a and 2a). After sintering for 20 h at 300 °C under F_2 atmosphere, peaks assignment shows that the powders are constituted of two crystallized phases consistent with YF_3 and $LiYF_4$ for yttrium samples (Fig. 1b) and with GdF_3 and LiF for gadolinium samples (Fig. 2b). After further treatment for 20 h at 550 °C under F_2 atmosphere, single and well crystallized phases of $LiYF_4$ and $LiGdF_4$ with inverse scheelite structure are obtained (Figs. 1c and 2c) in accordance with the diffraction patterns of the reference data ($LiGdF_4$: JCPDS-file 27-1236; $LiYF_4$: JCPDS-file 81-2254).

In order to check that all the organic parts have been removed from the sol–gel-derived samples after heating

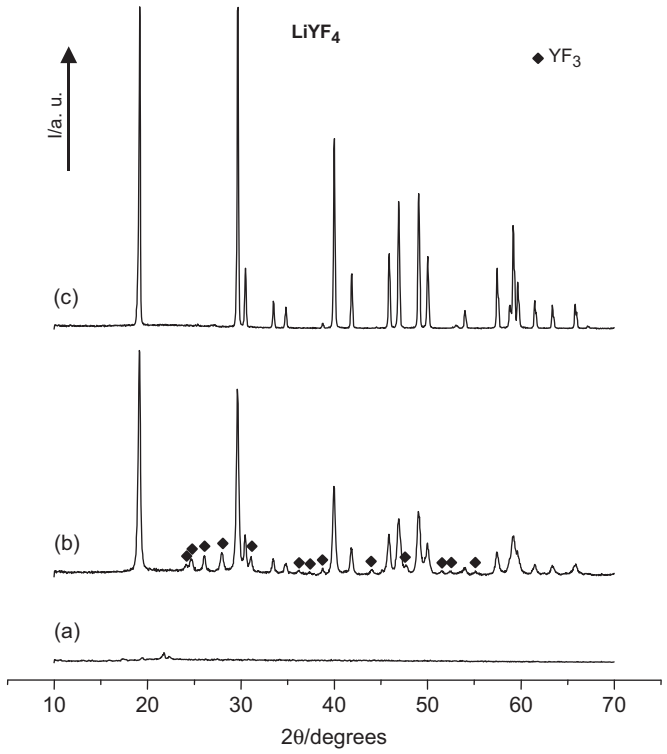

Fig. 1. XRD patterns recorded from powders of lithium yttrium fluoride (a) as-prepared and after sintering for 20 h under F_2 (b) at 300 C and (c) at 550 °C.

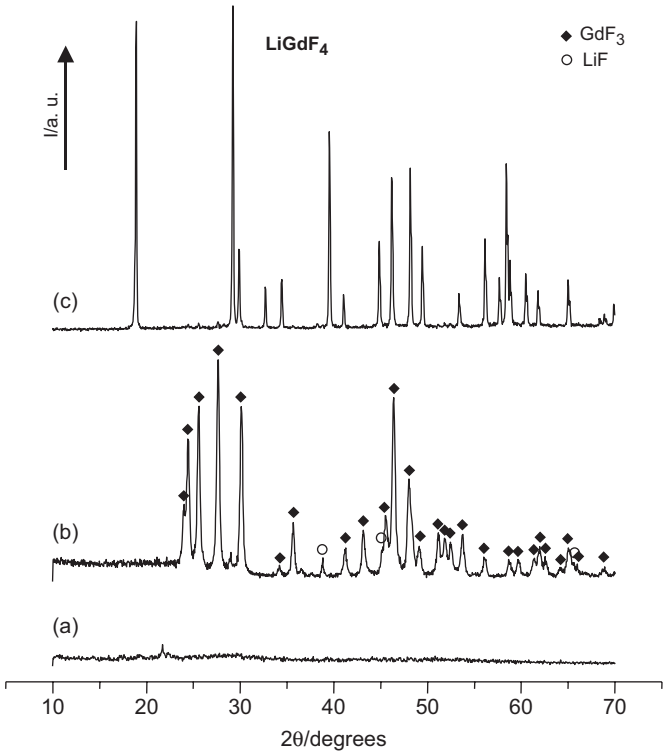

Fig. 2. XRD patterns recorded from powders of lithium gadolinium fluoride (a) as-prepared and after sintering for 20 h under F_2 (b) at 300 °C and (c) at 550 °C.

treatment, an infrared spectroscopy study was performed in the 4000–400 cm^{-1} range. Only the FTIR spectra recorded from the lithium yttrium fluoride powders are presented in Fig. 3 since FTIR spectra are nearly identical for the gadolinium samples.

The spectrum recorded from the xerogel sample (Fig. 3a) exhibits characteristic signals of the organic compounds utilized or formed through the sol–gel synthesis i.e. isopropanol, 1,1,1-trifluoro-5-methyl-2,4-hexanedione and lithium yttrium isopropoxides. The broad band ranging from 3000 to 3750 cm^{-1} is ascribed to O–H stretching vibrations in residual alcohol used as solvent and trapped within the powder. Next to that, three vibration modes located at 2972, 2936 and 2878 cm^{-1} are attributed to C–H stretching vibrations in CH_3 and CH groups. Regarding the sharp and strong bands between 1700 and 1640 cm^{-1}, they can be assigned to C = O stretching vibrations resulting from the β-diketone used as in-situ fluorine agent and metallic acetylacetonate groups obtained by reaction with yttrium isopropoxide. Below 1600 cm^{-1}, attribution of remaining bands is not evident, but one can say that they are due to vibrations of C–O, C–C, C–H and CF_3 bondings. After sintering at 300 °C for 20 h under F_2 atmosphere, most vibration bands of organic groups have been removed as shown on Fig. 3b and only the bands related to the fluoride lattice are observed below 600 cm^{-1}. The last spectrum (Fig. 3c), recorded from the $LiYF_4$ crystallized sample heat-treated at 550 °C under the same conditions, reveals the absence of organic residue. On the

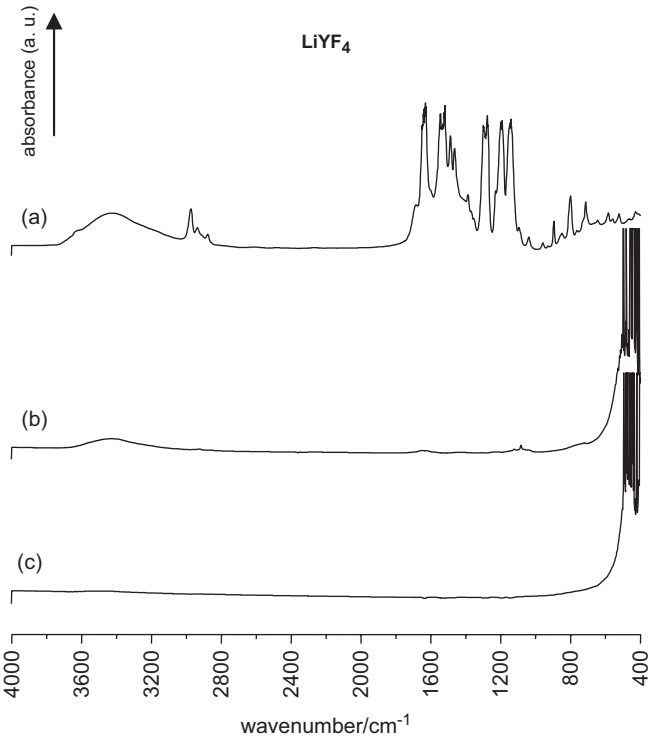

Fig. 3. FTIR spectra recorded from powders of lithium yttrium fluoride (a) as-prepared and after sintering for 20 h under F_2 (b) at 300 °C and (c) at 550 °C.

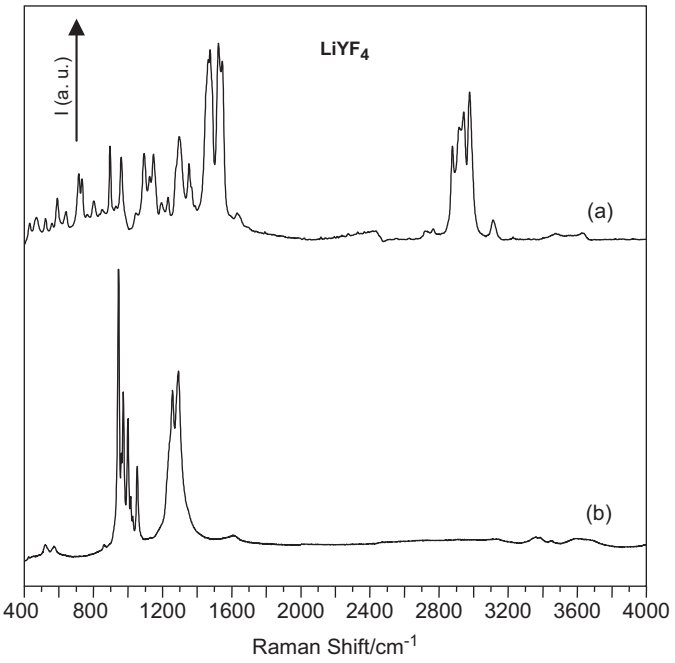

Fig. 4. Raman spectra recorded from powders of lithium yttrium fluoride (a) as-prepared and (b) after sintering at 550°C for 20 h under F_2 atmosphere.

basis of these results, the sintering process under fluorine atmosphere is proved to be suitable so as to remove all the organic residual parts as well as the hydroxyl groups, which would affect for instance the luminescence properties of rare-earth-doped $LiGdF_4$ and $LiYF_4$ phosphors. Achievement of free-OH powders was confirmed by another work [12] demonstrating the absence of Eu–O charge transfer band in the excitation spectrum of $LiGdF_4$:Eu^{3+} prepared with the same synthesis way.

Such a result was also evidenced by Raman spectroscopy. In Fig. 4 are displayed the Raman spectra related to $LiYF_4$ and recorded from xerogel sample as well as from the crystallized one sintered at 550 °C. The amorphous powder (Fig. 4a) exhibits mainly peaks assigned to organic groups. In particular, in the range lying from 2900 to 3100 cm^{-1}, the presence of strong peaks is attributed to C–H stretching vibrations in alkoxides and residual isopropanol. Signal due to O-H stretching vibrations is weak, therefore it does not appear significantly. Strong bands located between 1420 and 1580 cm^{-1} can be ascribed to acetonate stretching vibrations arising from the β-diketone 1,1,1-trifluoro-5-methyl-2,4-hexanedione used as in-situ fluorination reagent. After annealing for 20 h at 550 °C under F_2 atmosphere (Fig. 4b), all the peaks related to organic parts have been removed. Remaining signals are characteristic of tetrafluoride compounds as already observed in works undertaken by Karim et al. [23].

To investigate the structural arrangement from the amorphous xerogel sample to the well-crystallized rare-earth tetrafluoride powder when increasing the sintering temperature, ^{19}F NMR technique was used to characterize the local environment of fluorine atoms. Because of Gd^{3+} ions, the NMR measurements were carried out only for lithium yttrium fluoride specimen. Indeed, due to a number of uneven electrons, Gd^{3+} ions [Xe] $4f^7$ exhibit intrinsic magnetic moments and paramagnetism at ambient temperature. The effect of paramagnetic centers (PC) on nuclear spin relaxation has been the subject of many studies [24–26]: coupling between nuclear spin and unpaired electron spin (even in small concentration, because the electron has a much larger gyromagnetic ratio) produces a very effective channel for nuclear spin-lattice relaxation. At high amount of PC, the nuclear relaxation can be too short to be measured and the NMR line drastically decreases and widens or disappears.

The room temperature ^{19}F NMR spectra of sol–gel-based xerogel and samples annealed at 300 and 550 °C were compared in Figs. 5 and 6 to the one recorded from $LiYF_4$ powder synthesized by classical solid-state reaction ($LiF–YF_3$ at 600 °C under F_2). Two treatment durations at 300 °C were applied: 2 and 20 h. Apart from the xerogel spectrum, the static spectra (Fig. 5) exhibit a very broad line centered near −90 ppm/$CFCl_3$. The full widths at half maximum (FWHM) are equal to 2 kHz for the xerogel and 60 kHz for $LiYF_4$ whatever the sintering and synthesis conditions. For these latter samples, homonuclear ^{19}F–^{19}F dipolar coupling explains this broadening. Moreover, the top of the resonance is much flatter than that of a Gaussian curve. Such line shape is characteristic for a convolution of Gaussian curve with a rectangular envelope [27]. Similar

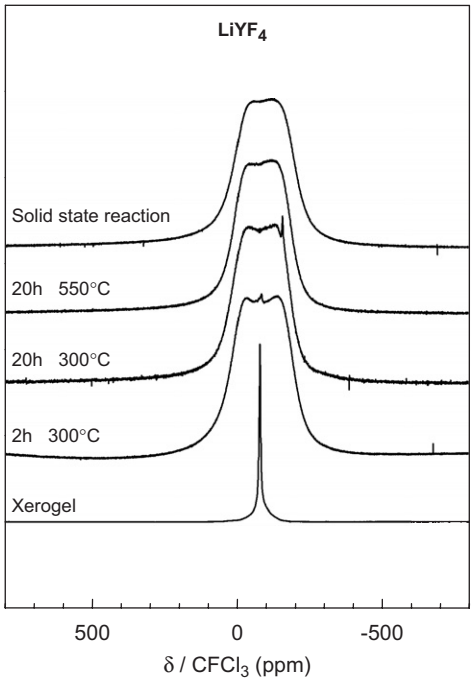

Fig. 5. ^{19}F NMR static spectra recorded at RT from sol–gel-derived $LiYF_4$ powders sintered at different temperatures and $LiYF_4$ sample obtained by solid-state reaction.

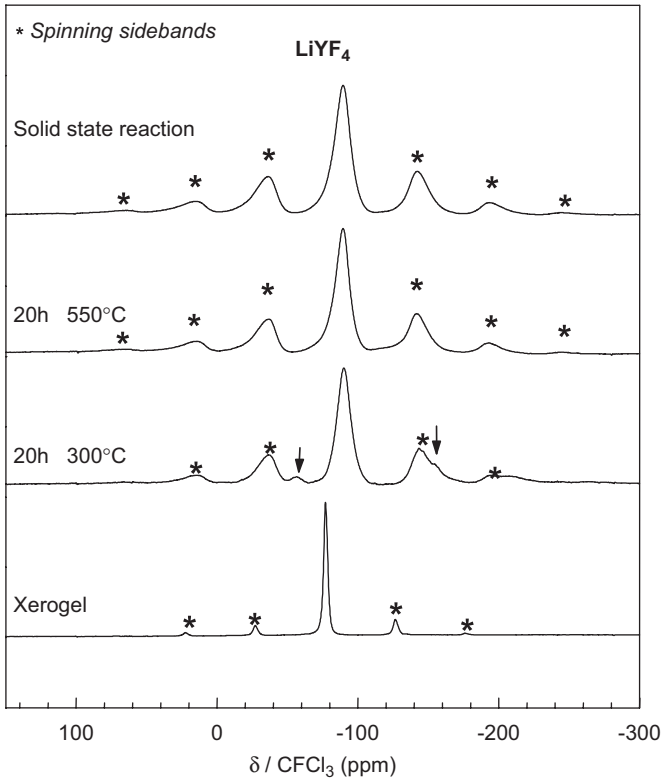

Fig. 6. ^{19}F NMR MAS spectra recorded at RT from sol–gel-derived $LiYF_4$ powders sintered at different temperatures and $LiYF_4$ sample obtained by solid-state reaction.

shapes have already been obtained for instance from inorganic fluorides such as LiF [28], CaF_2 [27,29] or powdered gypsum [30] although these solids have no separate groups of nuclei (i.e. identical neighboring for fluorine atoms). In fact, the dipole–dipole coupling of a given spin with others may be described as a sum of two statistically independent parts: the nearest neighbors and the spins in the rest of the crystal, resulting in the rectangular shape and in a Gaussian distribution function, respectively.

As shown in Fig. 6, by the presence of a single line centered at −90 ppm, the MAS spectra (with spinning speed of 14 kHz) of the various $LiYF_4$ samples confirm that all the ^{19}F nuclei are similar in accordance with the structural model [16]. The FWHM decreases from 60 to 4 kHz for sol–gel-derived $LiYF_4$ and for $LiYF_4$ obtained by solid-state reaction.

The homonuclear coupling is maximized in well-organized rigid matrix. Starting from disordered xerogel, for which the NMR resonance at −79 ppm is assigned to $-CF_3$ groups from initial 1,1,1-trifluoro-5-methyl-2,4-hexanedione, the sintering results in the crystallization and then in the increase of the dipolar coupling leading to a broadening line. This structural arrangement is nearly achieved as soon as 2 h at 300 °C under F_2 since the FWHM of the line remains constant whatever the sample. Very low additional lines are present on the static spectra of $LiYF_4$ prepared at 300 °C for 2 and 20 h; the corresponding chemical shifts are −79 and −160 ppm, respectively. The first line is assigned to residual xerogel whereas the second is attributed to fluorinated carbons, which are formed during the sintering of the organic precursor under fluorine gas. C-F bonds can be formed at this temperature under F_2 atmosphere explaining the weak line at −160 ppm. A further sintering at 550 °C results in the removal of these fluorinated carbons by reaction with fluorine gas forming volatile CF_4, C_2F_6, etc. The origin of the line at −57 ppm is unambiguous. On the basis of the XRD characterization, which reveals the presence of YF_3 after sintering at 300 °C and then its disappearance when the sample is treated at 550 °C, this resonance was assigned to yttrium trifluoride. Furthermore, YF_3 spectrum (not shown here) recorded with a spinning speed of 14 KHz exhibits an isotropic line at 57.2 ppm and a shoulder at 67.2 ppm confirming then our assignment.

The change of the ^{19}F Spin-lattice relaxation time T_1 confirms the structural evolution since its value increased from 1.67 to 3.15 s after the sintering at 550 °C. As a result, the fluoride matrix becomes more rigid and the nuclear relaxation is slowed down.

In accordance with XRD analysis, NMR characterization reveals the strong similitude between sol–gel-derived $LiYF_4$ and $LiYF_4$ prepared by direct solid-state reaction. Furthermore, it is proved that a sintering treatment at 550 °C is necessary both to convert all the xerogel in $LiYF_4$ and to remove fluorinated carbons, which are formed by side reactions under fluorine gas.

The Gd L_3-edge and Y K-edge EXAFS spectra of samples and fluoride references are shown in Figs. 7a and 7c, respectively. Their corresponding PRDFs uncorrected

from phase shift are displayed in Figs. 7b and d, respectively. From these patterns, one can see only one coordination shell for both xerogels, which is characteristic of amorphous compounds or highly disordered environments. After a 300 °C heating treatment, the sample containing gadolinium exhibits EXAFS oscillations and a PRDF very similar to that of GdF_3 whereas the yttrium-based sample provides data very close to those obtained from the powder annealed at 550 °C, which has been identified by XRD as $LiYF_4$ phase. In order to assess fractional contributions of each fluoride phase, linear least-squares fitting has been carried out on k^3-weighted

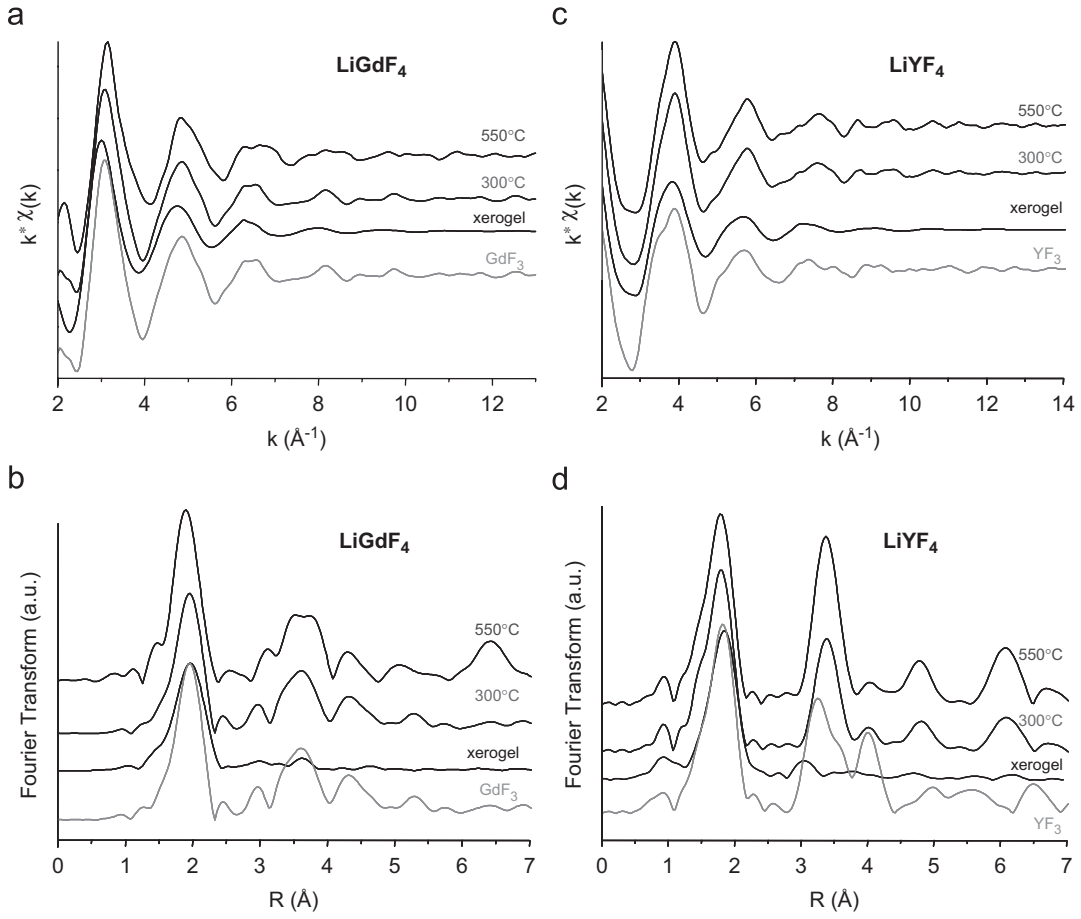

Fig. 7. (a) Gd L_3-edge $k\chi(k)$ EXAFS oscillation and (b) its corresponding Fourier Transform uncorrected from phase shift for gadolinium-based samples: xerogel, samples annealed at 300 and 550 °C and GdF_3; (c) Y K-edge $k\chi(k)$ EXAFS oscillations and (d) its corresponding Fourier transform uncorrected from phase shift for yttrium-based samples: xerogel, samples annealed at 300 and 550 °C and YF_3.

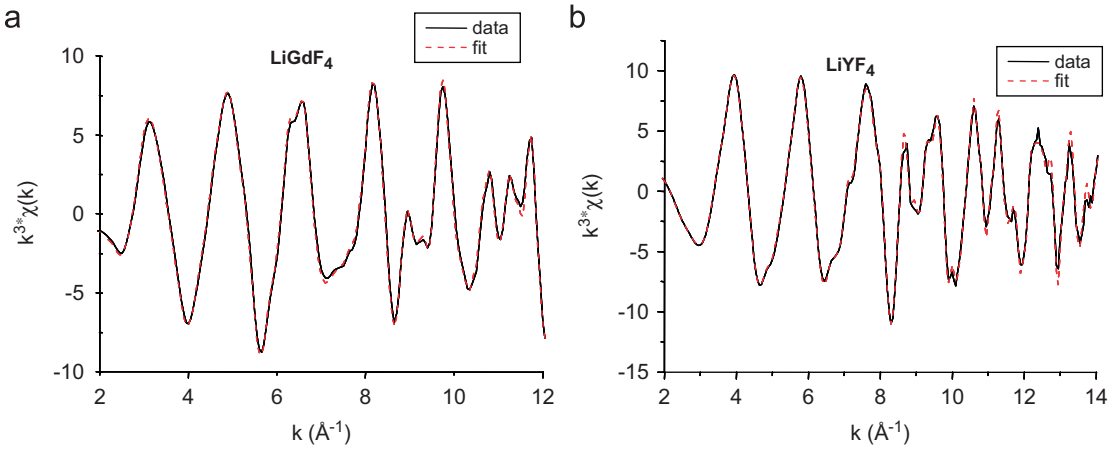

Fig. 8. Experimental (solid lines) and linear least-squares fittings (dashed lines) of $k^3\chi(k)$ EXAFS oscillations for (a) gadolinium-based and (b) yttrium-based fluorides sintered at 300 °C.

experimental EXAFS spectra of these two samples. Corresponding results presented in Fig. 8 and Table 1 are consistent with XRD analysis (Figs. 1 and 2). Indeed, after a 300 °C heating treatment, the compound elaborated from gadolinium chloride consists of 88% of GdF_3 whereas the one synthesized from yttrium salt contains 75% of $LiYF_4$. Finally, samples sintered at 550 °C exhibit spectra in accordance with the crystal structure descriptions of $LiYF_4$ [16] and $LiGdF_4$ [17], as well as with a previous EXAFS study led on $LiYF_4$–$LiREF_4$ solid solutions [31].

Table 1
Results of linear least-squares fittings of samples annealed at 300 °C

$LiGdF_4$ series	$LiYF_4$ series
88% GdF_3	14% YF_3
	75% $LiYF_4$
12% amorphous	11% amorphous
$\chi^2_V = 0.05$	$\chi^2_V = 0.27$

Structural parameters of xerogels and samples annealed at 300 and 550 °C were obtained by fitting the first coordination shell, which was filtered in the 1.1–2.6 Å range. From linear fitting results regarding PRDF obtained in the k range, data of the sample containing gadolinium and sintered at 300 °C were fitted with respect to GdF_3

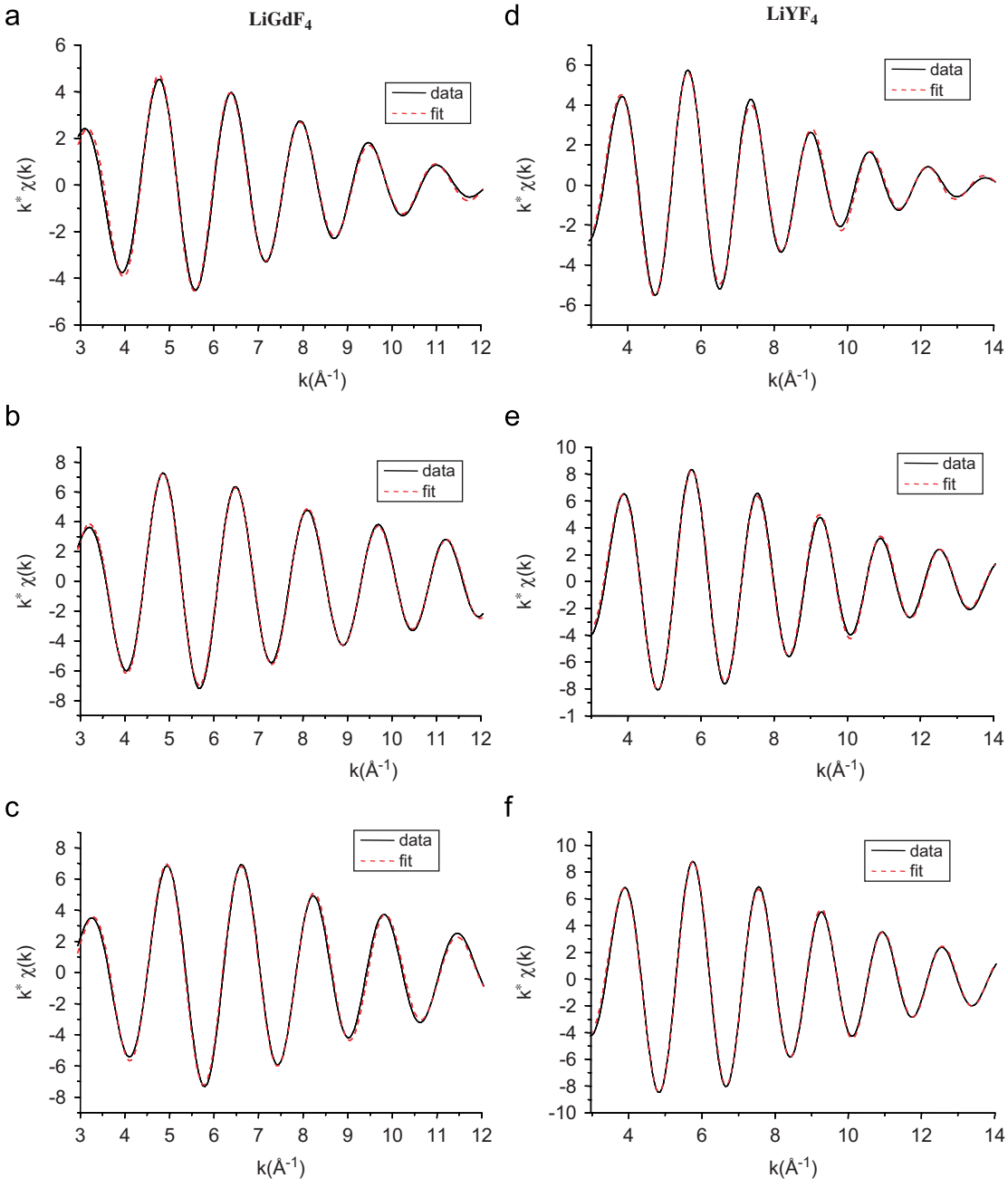

Fig. 9. Experimental (solid lines) and fitted (dashed lines) first-shell filtered EXAFS spectra for (a–c) gadolinium-based and (d–f) yttrium-based materials: xerogels (a, d) and samples annealed at 300°C (b, e) or 550°C (c, f).

Table 2
Structural parameters determined from the EXAFS data recorded at Gd L_3 and Y K edges. Data between brackets correspond to the literature [16]

Samples		N	R (Å)	σ (Å)	R_F (%)
$LiGdF_4$–Gd K-edge	xerogel	7.3	2.39	0.09	0.41
	300 °C	5.7	2.33	0.07	0.48
		1.9	2.40	0.01	
		0.9	2.54	0.02	
	500 °C	3.9	2.27	0.03	0.45
		4.1	2.38	0.04	
	GdF_3	6	2.33	0.06	0.16
		2	2.40	0.01	
		1	2.54	0.02	
$LiYF_4$–Y K-edge	xerogel	6.1	2.33	0.09	0.68
	300 °C	3.9	2.26	0.06	0.49
		4.1	2.32	0.09	
	500 °C	3.8 (4)	2.245 (2.44)	0.05	0.42
		4.3 (4)	2.321 (2.297)	0.08	

single scattering paths generated ab initio whereas other samples were compared with $LiGdF_4$ or $LiYF_4$ phases.

Results of fits and structural parameters are gathered in Fig. 9 and Table 2, respectively. Regarding samples sintered at 550 °C (Figs. 9c and f), satisfying fit of the EXAFS spectra was obtained on the assumption of two groups of four fluorine atoms at R_1 (2.24 Å) and R_2 (2.32 Å) distances as it is described in the crystallographic structure of $LiYF_4$ [16,32]. Bond lengths related to $LiYF_4$ (Table 2) are similar to those mentioned in the literature, even though the second Y–F is slightly longer than that determined from crystallographic data (2.32 Å instead of 2.30 Å). This can be related to the fit accuracy (1% for R). Coordination numbers (about two groups of four fluorine atoms) are in accordance with the XRD results.

Samples annealed at 300 °C (Figs. 9b and e) are already well organized: yttrium fluoride shows structural parameters very similar to those of $LiYF_4$ and gadolinium fluoride exhibits almost the same data than those of GdF_3. These fits are well consistent with previous remarks and with XRD and NMR studies. Data determined for xerogels (Figs. 9a and 9d) indicate primitive arrangement around lanthanide atoms represented by environments consisting of about seven and six fluorine atoms with distances in agreement with GdF_3 structure ($R = 2.39$ Å which is an intermediate value between 2.33, 2.40 and 2.54 Å) and $LiYF_4$ structure ($R = 2.32$ Å instead of 2.24 and 2.30 Å) for gadolinium and yttrium based fluorides, respectively.

Regarding the microstructural study, samples morphology was investigated by SEM. Thus, SEM pictures of as-prepared and 550 °C annealed $LiGdF_4$ samples were recorded to evidence the effect of the sintering treatment on morphological features. Resulting xerogel micrograph, shown in Fig. 10, consists of micrometric agglomerated plates of inhomogeneous size. After thermal treatment under fluorine atmosphere for 10 h at 550 °C, the powder is composed of small, spherical and coalescent particles. This peculiar shape results from crystallization and aggregation processes which have occurred at 550 °C. When increasing the annealing time up to 20 h, particles agglomerate and

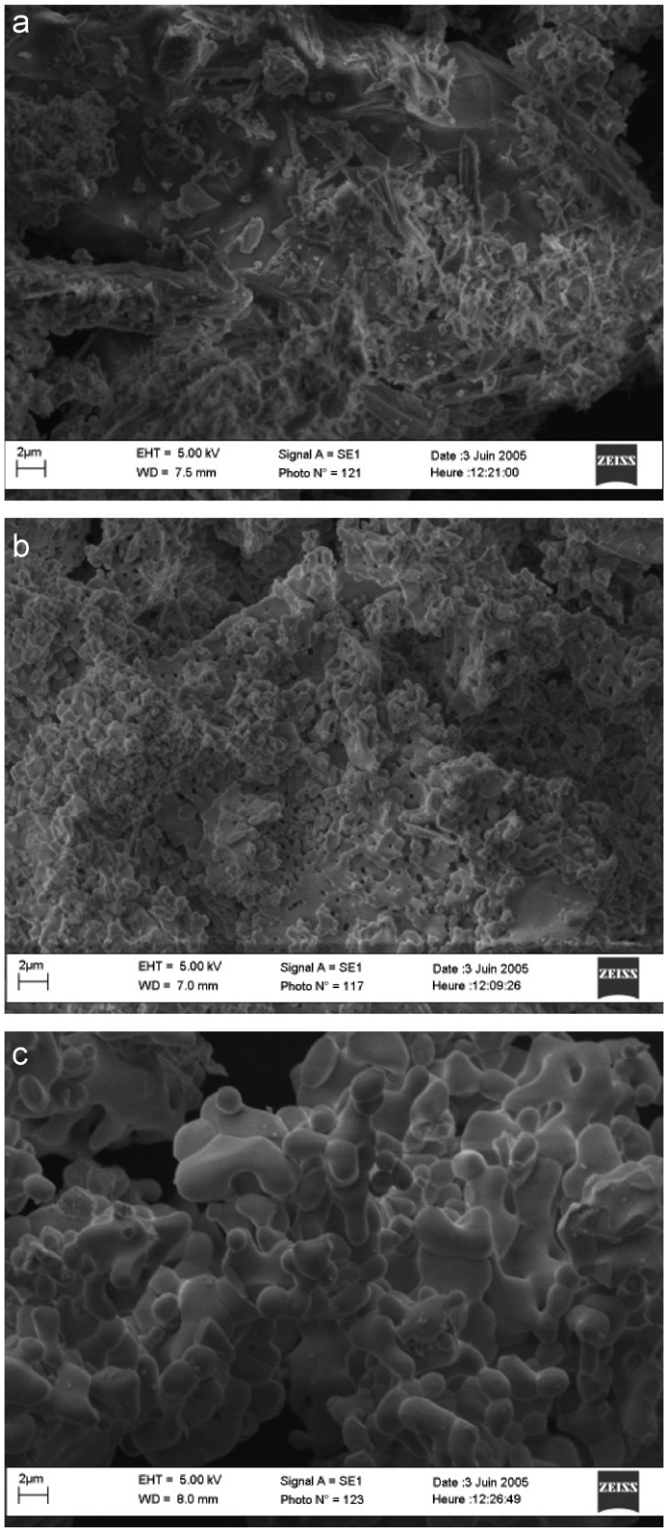

Fig. 10. SEM images (× 2.5 K) of lithium gadolinium fluoride powders (a) as-prepared and after heat treatment at 550 °C under F_2 atmosphere (b) for 10 h and (b) 20 h.

become much larger as shown in Fig. 10c. As a result, one can say that the powder microstructure depends significantly on the sintering conditions.

4. Conclusion

Pure and well-crystallized powders of $LiYF_4$ and $LiGdF_4$ were successfully synthesized by the sol–gel process. IR and Raman spectroscopies have demonstrated the absence of organic residues in resulting fluorides while ^{19}F NMR and XAS measurements have confirmed the formation of well-organized structure as soon as 300 °C even though a 550 °C treatment is needed to insure complete crystallization of $LiYF_4$ and $LiGdF_4$. Such a result is of interest since fluoride lattices are largely used as host materials for phosphors so that any presence of organic residue would make drastically drop the efficiency. Moreover, it has been shown that sol–gel-derived $LiYF_4$ powder is structurally as well-organized as $LiYF_4$ prepared by conventional solid-state synthesis. The optical properties of $LiGdF_4$:Eu^{3+} and $LiYF_4$:Er^{3+} have been studied [12] and evidenced the advantages of the sol–gel process for preparing doped materials.

Furthermore, samples microstructure was proved to be very sensitive to the thermal treatment undergone. This feature has to be taken into account since it could greatly affect the properties of fluoride powders whatever their future applications.

One of the main advantages of sol–gel process over solid-state reaction is the ability of preparing coatings from the alkoxide solution. We have already succeeded in preparing $LiYF_4$ coatings by spray technique [10]. Such achievement should open up the possibility to produce versatile-shaped fluorides and consequently to widen their application fields as well as to increase their efficiencies.

Acknowledgments

The authors are grateful to the European Community for having financially supported the XAS measurements carried out at Elettra (Contract RII3-CT-2004-506008 (IA-SFS)).

References

[1] C.J. Brincker, G.W. Scherer, Sol–Gel Science, Academic Press, New York, 1990.
[2] L.L. Hench, K. West, J. Chem. Rev. 90 (1990) 33.
[3] C. Sanchez, J. Livage, New J. Chem. 14 (1990) 513.
[4] M. Guglielmi, G. Carturan, J. Non-Cryst. Solids 100 (1988) 16.
[5] C. Fouassier, Advanced Inorganic Fluorides—Synthesis, Characterization and Applications, Elsevier, Amsterdam, 2000.
[6] F. Okada, S. Togawa, K. Ohta, J. Appl. Phys. 75 (1994) 49.
[7] C.M. Combes, P. Dorenbos, C.W.E. van Eijk, C. Pedrini, H.W. Den Hartog, J.Y. Gesland, P.A. Rodnyi, J. Lumin. 71 (1997) 65.
[8] S. Fujihara, M. Tada, T. Kimura, Thin Solid Films 304 (1997) 252.
[9] S. Fujihara, S. Ono, Y. Kishiki, M. Tada, T. Kimura, J. Fluorine Chem. 105 (2000) 65.
[10] D. Boyer, R. Mahiou, Chem. Mater. 16 (2004) 2518.
[11] D. Boyer, H. Kharbache, R. Mahiou, Opt. Mater. 28 (2006) 53.
[12] S. Lepoutre, D. Boyer, R. Mahiou, Opt. Mater. 28 (2006) 592.
[13] S.M. Webb, Phys. Scripta 115 (2005) 1011.
[14] B.J. Ravel, Synchrotron Rad. 8 (2001) 314.
[15] A.L. Ankudinov, B. Ravel, J.J. Rehr, S.D. Conradson, Phys. Rev. B 58 (1998) 7565.
[16] E. Garcia, R.R. Ryan, Acta Crystallogr. C 49 (1993) 2053.
[17] Brunton et al., Oak Ridge International Laboratory, Rep. ORNL (US), 1965, p. 3761.
[18] A.K. Cheetham, N. Norman, Acta Chem. Scand. A 28 (1974) 55.
[19] A. Zalkin, D.H. Templeton, J. Am. Chem. Soc. 75 (1953) 2453.
[20] B. Toner, A. Manceau, S.M. Webb, G. Sposito, Geochim. Cosmochim. Acta 70 (2006) 27.
[21] M.J. Newville, Synchrotron Rad. 8 (2001) 322.
[22] S. Daviero, L. Montagne, G. Palavit, G. Mairesse, S. Belin, V. Briois, J. Phys. Chem. Solids 64 (2003) 253.
[23] M. Karim, Ph.D. Thesis, University of Blaise Pascal (Clermont II), 1996.
[24] W.E. Blumberg, Phys. Rev. 119 (1960) 79.
[25] D. Tse, S.R. Hartmann, Phys. Rev. Lett. 21 (1968) 511.
[26] M.R. McHenry, B.G. Silbernagel, Phys. Rev. B 5 (1972) 2958.
[27] A. Abragam, The Principles of Nuclear Magnetism, Oxford University Press, London, 1961.
[28] U. Groß, S. Rüdiger, M.-R. Grimmer, E. Kemnitz, J. Fluorine Chem. 115 (2002) 1993.
[29] E.M. Purcell, N. Bloembergen, R.V. Pound, Phys. Rev. 70 (1946) 988.
[30] G.E. Pake, J. Chem. Phys. 16 (1948) 327.
[31] M.E.G. Valerio, A.V. Chadwick, J.F. De Lima, I.M. Ranieri, Radiat. Eff. Defects Solids 157 (2002) 1173.
[32] B. Minisini, Q.A. Wang, F. Tsobnang, J. Phys.: Condens. Matter 17 (2005) 4953.